Received: 31 January 2019 | Revised: 13 July 2020 | Accepted: 13 July 2020

DOI: 10.1002/jrs.5979

SPECIAL ISSUE - RESEARCH ARTICLE

Journal of RAMAN SPECTROSCOPY WILEY

Micro-Raman study of crichtonite group minerals enclosed into mantle garnet

Taisia Alifirova[1,2] | **Dmitriy Rezvukhin**[1] | **Evgeny Nikolenko**[1,3] | **Lyudmila Pokhilenko**[1] | **Pavel Zelenovskiy**[4] | **Igor Sharygin**[1,5] | **Andrey Korsakov**[1] | **Vladimir Shur**[4]

[1]Sobolev Institute of Geology and Mineralogy, Siberian Branch, Russian Academy of Sciences, Novosibirsk, Russian Federation

[2]Department of Lithospheric Research, University of Vienna, Vienna, Austria

[3]Geo-Scientific Research Enterprise ALROSA (PJSC), Mirny, Russian Federation

[4]Institute of Natural Sciences and Mathematics, Ural Federal University, Ekaterinburg, Russian Federation

[5]Institute of the Earth's Crust, Siberian Branch, Russian Academy of Sciences, Irkutsk, Russian Federation

Correspondence
Taisia Alifirova, Sobolev Institute of Geology and Mineralogy, Siberian Branch, Russian Academy of Sciences, 3 Academician Koptyug Avenue, Novosibirsk 630090, Russian Federation.
Email: taa@igm.nsc.ru; taisia.alifirova@univie.ac.at

Funding information
Russian Science Foundation, Grant/Award Number: 18-77-10062

Abstract

We report the first comprehensive micro-Raman study of crichtonite group minerals (CGM) as inclusions in pyropic garnet grains from peridotite and pyroxenite mantle xenoliths of the Yakutian kimberlites as well as in garnet xenocrysts from the Aldan shield lamprophyres (Russia). The CGM form (i) morphologically oriented needles, lamellae, and short prisms and (ii) optically unoriented subhedral to euhedral grains, either single or intergrown with other minerals. We considered common mantle-derived CGM species (like loveringite, lindsleyite, and their analogues), with Ca, Ba, or Sr dominating in the dodecahedral A site and Zr or Fe in the octahedral B site. The Raman bands at the region of 600–830 cm^{-1} are indicative of CGM and their crystal-chemical distinction, although the intensity and shape of the bands appear to be dependent on laser beam power and wavelength. The factor-group analysis based on the loveringite crystal structure showed the octahedral and tetrahedral cation groups with 18*f* and 6*c* Wyckoff positions, namely, dominantly TiO_6 and to a lower extent CrO_6, MgO_4, and FeO_4 groups, to be the major contributors to the Raman spectral features. The ionic groups with dodecahedral (M0) and octahedral (M1) coordination are inactive for Raman scattering while active in infrared absorption. A number of observed Raman modes in the CGM spectra are several times lower than that predicted by the factor group analysis. The noticed broadening of modes in the CGM Raman spectra may result from a combining of bands at the narrow frequency shift regions. Solid solution behavior, luminescence, and partial metamictization of the CGM may exert additional influence on the Raman band shape. The Raman spectral features showed CGM to be accurately identified and distinguished from other Ti-, Fe-, Cr-, and Zr-containing oxides (e.g., ilmenite or those of spinel and magnetoplumbite groups) occurring as accessory mantle minerals.

KEYWORDS
crichtonite group minerals, mantle xenoliths, oriented inclusions, pyrope, Raman spectroscopy

1 | INTRODUCTION

Crichtonite group minerals (CGM) are oxides with large- and medium-sized cations (Nickel–Strunz Classification, 04.CC.40). Their common structural formula $^{XII}A^{VI}B^{VI}C_{18}{}^{IV}T_2(\Phi)_{38}$ reflects a great variability of chemical compositions.[1,2] The most abundant cations are ^{XII}A = Ba, K, Pb, Sr, La, Ce, Na, Ca; ^{VI}B = Mn, Y, U, Fe, Zr, Sc; $^{VI}C_{18}$ = Ti, *Fe*, *Cr*, V, *Nb*, *Mn*, *Al*; $^{IV}T_2$ = Fe, Mg, Zn; and anions are Φ = O, (*OH*); ions and radicals not known to prevail in natural samples are italicized. The minerals are characterized by a layer structure and a highly complex composition.[3] However, only Ti, Fe, and O are systematically present.[4] The currently used nomenclature of the CGM is based upon the combination of dominant cations in the sites ^{XII}A, ^{VI}B, ^{VI}C, and ^{IV}T.[5] It describes several solid solutions and suggests naming minerals with respect to a certain combination of prevailing cations (Table 1).

The CGM are known as accessory minerals in crustal (e.g., Mills et al[11] and Filho et al[13]), upper mantle (e.g., Rezvukhin et al[24] and Grégoire et al[26]), and meteoritic rocks.[27] They also occur in the heavy mineral concentrates of deep-sourced mantle-derived rocks[16] and a heavy fraction of clastic sediments[28,29] due to their resistance to weathering and a high density. The origin of CGM is related to variable magmatic, metasomatic, metamorphic, and hydrothermal processes (e.g., other studies[4,23,24,30-34]). It is noteworthy that crystalline phases with the crichtonite structure have also received significant attention due to their suitability as a storage media for high-level radioactive waste, especially radionuclides with large ionic radii.[35,36]

Regarding the CGM in mantle rocks, the species with mainly Ca, K, and Ba in the A position and Zr and Fe in the B position appear to be the most abundant (see review in Rezvukhin et al[24]). These species are also characteristically enriched in Cr and Mg, whereas inclusions in Cr-bearing pyropic garnet additionally contain comparably high Al.[24,37,38] The Sr- and Pb-rich varieties with U, Y, and Mn in the B position and substantial Zn in the T position are not found as typical of mantle associations.[4,23,37] However, the study of mantle CGM shows possibilities for finding new species in the group with a highly variable A-site cation set.[23,24,39] According to the current classification, some CGM species found in upper mantle rocks still do not have mineral names.[4,5] Thus, to acquire a wider study of CGM, their careful identification is needed.

However, the identification of CGM in a mantle material is mainly confined to the measurements of their composition by means of electron microprobe and scanning electron microscope (SEM), whereas the structural data are usually challenging to obtain, especially taking into account a common small size of the grains (e.g., other studies[37,40-42]). In light of the aforementioned, the micro-Raman spectroscopic technique serves as a helpful tool for the express and accurate diagnostics of CGM, which is highly applicable to a study of inclusions in mantle minerals.

The known works considering the Raman spectra of CGM are focused on the study of natural or synthetic materials. Raman data are presented for natural crichtonite, cleusonite, davidite (reference numbers from RRUFF Project database[25] are given in Table 1), as well as for gramaccioliite-(Y),[43] dessauite-(Y),[9] lindsleyite-(Fe),[22] and synthetic CGM of lindsleyite-mathiasite (LIMA) solid solution series.[18] The attempts to obtain the Raman spectrum of paseroite have also been mentioned.[11] However, loveringite and its Sr-, Na-, Cr-, and Mg-bearing counterparts usually described in mantle rocks have not been yet characterized by the micro-Raman spectroscopic technique. It is crucial to obtain and interpret the information on the Raman spectra of this group of Ti-Fe-Cr-oxides in order to comprehend a variability of species and solid solutions of the CGM found in natural environments, particularly in mantle rocks.[16,44]

Here, we present the results of a new compositional and spectral study of mantle-derived CGM. Our primary intentions have been to consider correlations between the Raman spectrum features of CGM and their crystal-chemistry. We also report the analytical parameters and specific spectral features that we recommend to regard when obtaining and interpreting the Raman spectra of CGM. The data allow identifying these minerals as inclusions or as separate grains in a rock matrix, particularly within thin intergrowths, both from mantle rocks (xenoliths) and their disintegrated fragments (xenocrysts), including those from heavy-mineral concentrate. The effective nondestructive approach to diagnose CGM in mantle rocks presented in this study offers a potential: (i) to make an extensive characterization of the CGM lithological confinement, (ii) to clarify the CGM genesis, and (iii) to delineate pressure-temperature-composition conditions, at which these minerals are stable in nature.

TABLE 1 Nomenclature of crichtonite group minerals, including unnamed and not approved members, and Raman data available for mineral species

Mineral	M0	M1	M2	M3–M5		Reference	Available Raman data	Raman studied material
IMA approved[a]								
Landauite	Na, Pb	Mn, Y	$(Zn, Fe)_2$	$(Ti, Fe, Nb)_{18}$	O_{38}	Grey and Gatehouse[6]		
Davidite-(La)	La, Ce, Ca	Y, HREE, U	$(Fe, Mg)_2$	$(Ti, Fe, Cr, V)_{18}$	O_{38}	Gatehouse and Grey[7]	R070698[b], R070697, R110047[8];	Natural
Davidite-(Ce)	Ce, La	Y, HREE, U	$(Fe, Mg)_2$	$(Ti, Fe, Cr, V)_{18}$	O_{38}	Gatehouse and Grey[7]	R120009	Natural
Crichtonite	Sr, Ba, Pb	Mn	$(Fe, Zn)_2$	$(Ti, Fe)_{18}$	O_{38}	Grey et al[3]	R060314, R090006	Natural
Dessauite-(Y)	Sr, Pb	Y, U	$(Fe, Zn)_2$	$(Ti, Fe)_{18}$	O_{38}	Orlandi et al[2]	[9]	Natural
Senaite	Pb, Sr	Mn	$(Fe, Zn)_2$	$(Ti, Fe)_{18}$	O_{38}	Wülser et al[4]	R060644	Natural
Gramaccioliite-(Y)	Pb, Sr	Y, Mn	$(Fe, Zn)_2$	$(Ti, Fe)_{18}$	O_{38}	Orlandi et al[43]	[9]	Natural
Cleusonite	Pb, Sr	U	$(Fe, Zn)_2$	$(Ti, Fe)_{18}$	O_{38}	Wülser et al[4]	R061019	Natural
Paseroite	Pb, Sr	Mn	$(Mn, Fe)_2$	$(V, Ti, Fe)_{18}$	O_{38}	Mills et al[11]		
Mapiquiroite	Sr, Pb	U, Y	Fe_2	$(Ti, Fe^{3+})_{18}$	O_{38}	Biagioni et al[12]		
Almeidaite	Pb	Mn, Y	Zn_2	$(Ti, Fe^{3+})_{18}$	$O_{36}(O, OH)_2$	Filho et al[13]		
Mianningite	□, Pb, Ce, Na	U, Mn	$Fe^{3+}{}_2$	$(Ti, Fe^{3+})_{18}$	O_{38}	Ge et al[14]		
Loveringite	Ca, LREE	Zr, Fe	$(Mg, Fe)_2$	$(Ti, Fe, Cr, Al)_{18}$	O_{38}	Gatehouse et al[15]	This study	Natural
Lindsleyite	Ba, K	Zr, Fe	$(Mg, Fe)_2$	$(Ti, Cr, Fe)_{18}$	O_{38}	Haggerty[16] and Zhang et al[17]	Konzett et al[18] and this study	Synthetic, natural
Mathiasite	K, Ba, Sr	Zr, Fe	$(Mg, Fe)_2$	$(Ti, Cr, Fe)_{18}$	O_{38}	Haggerty[16] and Gatehouse et al[19]	Konzett et al[18]	Synthetic
Not approved								
V-Fe-Sc-rich analogue of lindsleyite	Ba, Sr, Pb	Fe, Sc	Fe_2	$(Ti, V, Fe)_{18}$	O_{38}	Platt and Mitchell[20]		
V-Fe-Sc-rich analogue of crichtonite	Sr, Ba, Pb, Ca	Fe, Sc	Fe_2	$(Ti, V, Fe)_{18}$	O_{38}	Platt and Mitchell[20] and Potter and Mitchell[21]		
Lindsleyite-(Fe)	Ba, Ca	Fe, Zr	$(Mg, Fe)_2$	$(Ti, Cr, Fe, Al)_{18}$	O_{38}	Nikolenko et al[22] and this study	Nikolenko et al and[22] this study	Natural
Loveringite-(Fe)	Ca	Fe, Zr	$(Mg, Fe)_2$	$(Ti, Cr, Fe, Al)_{18}$	O_{38}	This study	This study	Natural
Sr-Na-Ca-Zr analogue of loveringite	Sr, Na	Ca, Zr	Fe_2	$(Ti, Fe)_{18}$	O_{38}	Barkov et al[23]		

(Continues)

TABLE 1 (Continued)

Mineral	M0	M1	M2	M3-M5		Reference	Available Raman data	Raman studied material
Sr-Fe analogue of loveringite	Sr, Ba, Ca	Fe, Zr	$(Mg, Fe)_2$	(Ti, Cr, Fe, Al)$_{18}$	O_{38}	Rezvukhin et al[24]	This study	Natural
Sr-Zr analogue of loveringite	Sr, Ca, Ba	Zr, Fe	$(Mg, Fe)_2$	(Ti, Cr, Fe, Al)$_{18}$	O_{38}	Rezvukhin et al[24]		
Na-rich loveringite-(Fe)	Ca, Na, LREE	Fe, Zr	$(Mg, Fe)_2$	(Ti, Fe, Cr, Al)$_{18}$	O_{38}	This study	This study	Natural

Note: With relation to a general CGM formula $^{XII}A^{V}B^{VI}C_{18}{}^{IV}T_2(\Phi)_{38}$, the cation sites are apportioned as M0 = A, M1 = B, M2 = T, and M3–M5 = C. The additional sites observed in some CGM,[1,2,12,19] that is, three octahedral sites (M6–M8) and one square pyramidal site (M9), are not considered. LREE and HREE are light and heavy rare earth elements (REE), respectively.

[a]Approved by the Commission on New Minerals, Nomenclature and Classification (CNMNC) of the International Mineralogical Association (IMA).

[b]Reference numbers are from RRUFF Project database.[25]

2 | ANALYTICAL TECHNIQUES

Petrographic and mineralogical examination of samples represented by mantle xenoliths ($n = 14$) and xenocrysts ($n = 4$) was performed at the Sobolev Institute of Geology and Mineralogy (IGM), Siberian Branch, Russian Academy of Sciences, Novosibirsk, Russia, and a substantial part of analytical work was accomplished there using the facilities of the Analytical Center for Multi-elemental and Isotope Research. Xenoliths were vacuum-filled with epoxy, cut, and double-side polished for thin sections (200–300 μm), whereas garnet xenocrysts were embedded into epoxy resin mounts and polished in preparation for analysis.

Polished thin sections and mounts were characterized by quick scanning and imaging using a Tescan MIRA 3 LMU SEM combined with an Oxford Instruments INCA Energy 450+ XMax-80 microanalysis system to obtain back-scattered electron (BSE) images and energy dispersive X-ray spectrometry (EDS) compositional data. To get EDS compositions, an accelerating voltage of 20 kV and counting times for each element of 20 or 60 s for point analyses and of 1,800 s for elemental mapping were used. Quantitative mineral electron microprobe (EMP) analyses were obtained using a JEOL JXA 8100 EMP analyzer equipped with wavelength dispersive X-ray spectrometry (WDS) system. The filament used provides a very stable beam current (0.3% for 12h) even at high currents (up to 10 μA) that is essential for precise minor and trace element measurements. Thin sections and mounts were sputter coated with 25–30 nm carbon films for EMP and SEM analytical study. Garnet compositions were collected using a 2-μm-beam size, a 100-nA-beam current, and an accelerating voltage of 20 kV. To measure Na in pyropes, a 10-kV accelerating voltage and a 30-nA-beam current were set. Counting times for each element were generally 20 s (10 s for peaks and 5 s for background from both sides), except for Ca (30 s). The following natural and synthetic standards (with lines taken in brackets) for garnet EMP analyses were used: pyrope O-145 (Mg$K\alpha$, Al$K\alpha$, Si$K\alpha$, Fe$K\alpha$), Cr-pyrope Ud-92 (Cr$K\alpha$), diopside (Ca$K\alpha$), glass GL-6 (Ti$K\alpha$), Mn-garnet (Mn$K\beta$), albite (Na$K\alpha$), and orthoclase (K$K\alpha$).

The EMP measurements of three garnet samples were fulfilled using a Cameca SX100 EMP analyzer at the University of Tennessee (Knoxville, USA). The operating conditions for them are placed into Appendix A. A 1-μm-beam size was taken to investigate CGM by EMP analysis. Standards and analytical conditions for CGM analyses are presented in Table S1.

The Cr$K\beta$ and Mn$K\alpha$ and V$K\beta$ and Ti$K\alpha$ peaks were analyzed with the laser-induced fluorescence (LIF)

spectrometer crystal to avoid superimposition of an abundant element line (Ti and Cr) with that of neighboring one (V and Mn). Overlap correction was applied to measurements to obtain Ce, Ba, and V concentrations, for which $0.0045 \times$ Ti, $0.00092 \times$ Ti, and $0.55 \times$ Cr wt% were subtracted from the Ce, Ba, and V contents of unknown samples, correspondingly. Correction of V to Cr concentration was needed to be done in case of lower-chromium samples (ca. less than 10 wt% of Cr_2O_3).

Prior to recalculation into oxides, raw analytical EMP data were processed using standard ZAF matrix correction routine. The analytical accuracy was about 1 rel.% for all major elements and about 5 rel.% for minor and trace elements. The detection limits (3σ criterion) are typically within 0.01%–0.03% at routine analytical conditions.

An overwhelming majority of morphologically oriented inclusions of CGM in garnet grains from mantle xenoliths have a small size, usually <5 μm in the shortest dimension, what in turn places limitations to a quantitative EMP composition study. The chemical analyses of nine CGM inclusions in garnets from six mantle xenoliths, with their SiO_2 content below 0.5 wt% (except for two grains with SiO_2 <0.9 wt%), are presented in the study (Table 2). They were no less than 5 μm across and about 50–100 μm long. The other analyses had to be excluded from the consideration because of a noticeable contribution from the host garnet (>1 wt% of SiO_2 content in CGM). Four CGM grains from the Aldan garnet xenocrysts were large enough for EMP analysis (>10 μm in diameter) and their SiO_2 content is even lower than 0.1 wt%.

The Raman measurements were performed at IGM by using a Horiba Jobin Yvon LabRAM HR800 spectrometer combined with a Nd:YAG laser (532-nm emission) and an Olympus BX41 microscope. The Raman spectra were recorded at room temperature in the backscattering geometry with a 100× objective lens (0.37-mm working distance, 0.9 numerical aperture) produced a focal spot diameter of ~1 μm, in the range of 60–4,000 cm^{-1} Raman shift. An air-cooled (Peltier cooled) charge-coupled device detector was utilized to register Raman signal. The collection time was usually 10 s, and 5 to 10 scans were accumulated. The spectral resolution for the recorded Stokes-side Raman spectra of ~2 cm^{-1} was achieved by usage of 1,800 grooves per millimeter gratings and 100 or 200 μm slits in order to get proper signal quality. Selected samples were also studied at the Ural Center for Shared Use «Modern Nanotechnology», Ural Federal University (Ekaterinburg, Russia) using a WITec Alpha300AR confocal Raman microscope equipped with a solid-state laser (488 nm), He-Ne laser (633 nm), and a microscope with a long working distance 100× objective lens (0.75 numerical aperture). The diffraction grating with 600 grids per millimeter was used, and a 10-s integration time along with 10 accumulations was set. The systems were calibrated using the 520.7 cm^{-1} Raman band of silicon before and after each experimental session. The full width at half maximum (FWHM) of the 520.7 cm^{-1} silicon band is 7.4 cm^{-1} for the LabRam and 3.9 cm^{-1} for the Alpha300AR. Background correction was performed by subtracting the minimum intensity of each spectrum, which was different for both systems.

3 | SAMPLE DESCRIPTION AND MINERALOGY

A set of mantle xenoliths (n = 14) from the Obnazhennaya, Udachnaya-East, and Mir kimberlite pipes (Kuoika, Daldyn, and Mirny kimberlite fields from Lower Olenyok, Daldyn-Alakit, and Malobotuobia regions, respectively), as well as garnet xenocrysts (n = 4) from lamprophyres of the Aldanskaya dike and Ogonek diatreme (Chompolo volcanic field, Aldan shield) have been studied (Table 3). Geographically, the sampled localities are situated in the Republic of Sakha (Yakutia), Russian Federation, whereas from the tectonic point of view, they belong to the Siberian craton. Lithologically xenoliths are represented by garnet (n = 10) and spinel-garnet (n = 4) varieties of lherzolites (n = 4), olivine websterites (n = 6), and websterites (n = 4). The detailed petrographic features for most of the xenoliths are described in Alifirova et al,[40] whereas several new samples (O-39, O-25, Ob113/12, Ob108/12, and Ob106/12) share similar peculiarities with those examined previously.

Pyropic garnet (up to 17 mm in diameter) from most of the xenoliths is notable due to the occurrence of shape-preferred oriented inclusions disposed along the <111> direction of the host, varying in morphology and size. Usually, these are rods, needles and platelets from 2–5 μm to 10–20 μm in thickness and 20–100 μm (rarely up to 500 μm) long. The inclusions are composed of rutile, Mg-rich ilmenite, clinopyroxene, CGM, olivine, and more rarely orthopyroxene, chromite, Na-Ca-amphiboles (Table 3). According to volume proportion estimates of inclusions, rutile in these samples is the most abundant mineral, although in some xenoliths (like UV223/09) its proportion is comparable with that of pyroxenes.[45] The needles and platelets in the examined pyropic garnets are monomineralic or polymineralic (Figure 1). In accordance with previous studies, shape-preferred orientation relationships of clinopyroxene and orthopyroxene, rutile, ilmenite, chromite, and olivine with the host garnet are consistent with their solid-state exsolution origin.[40,45]

TABLE 2 Summary of data on the studied samples containing CGM and other associated minerals as inclusions in garnet

Sample no.	Rock type	Variety	*T* (° C)	*P* (GPa)	CGM oriented/ unoriented	Other oriented inclusions
Obnazhennaya kimberlite, Kuoika field, Lower Olenyok region						
O-571	Lherzolite	Grt-Spl			+/–	Rt, Ilm, Cpx, Amp
O-39	Lherzolite	Grt	710	2.0	+/–	Rt, Ol, Ilm, Cpx
Ob113/12	Lherzolite	Grt-Spl	680	1.9	+/–	Rt, Ilm, Cpx
Ob106/12	Olivine websterite	Grt			+/–	Rt, Amp, Ilm, Opx
Ob108/12	Olivine websterite	Grt	720	1.9	+/–	Rt, Ilm,Ol,Cpx
O-25	Olivine websterite	Grt-Spl	670	1.8	+/–	Rt, Cpx
O-207	Olivine websterite	Grt	830	3.4	+/–	Rt, Ol, Cpx, Amp, Ilm
O-173	Websterite	Grt	830	2.8	+/–	Rt, Cpx, Ilm
O-264	Websterite	Grt			+/–	Rt, Cpx, Ilm
O-301	Websterite	Grt			+/–	Rt, Cpx, Ilm, Opx
O-550	Websterite	Grt	780	2.4	+/–	Rt, Ilm, Cpx
Udachnaya-East kimberlite, Daldyn field, Daldyn-Alakit region						
UV223/09	Olivine websterite	Grt	910	4.5	–/+	Cpx, Rt, Ol, Ilm, Opx
UV127/09	Olivine websterite	Grt	850	3.7	+/+	Cpx, Rt, Ilm
Mir kimberlite, Mirny field, Malobotuobia region						
M34/01	Lherzolite	Grt-Spl	740	2.4	+/+	Rt, Cpx, Opx, Ilm, Ol,Chr
Sample No.	Sample type	Grt type[a]	*T* (° C)	*P** (GPa)	CGM oriented/ unoriented	Associated mineral inclusions
Aldanskaya lamprophyre, Chompolo field, Aldan shield						
s21	Grt xenocryst	G9		2.9	–/+	Mgs, Cpx, Phl, Gr, (CGM +Ol), (CGM+Mgs)
1n11	Grt xenocryst	G9		2.5	+/–	Rt, Ilm, Amp, Ol, Gr, Cp, Phl, (Rt+Cpx+Ap+Mgs)
Ogonek lamprophyre, Chompolo field, Aldan shield						
s328	Grt xenocryst	G9		2.6	+/–	Rt, Ilm
s291	Grt xenocryst	G9		2.8	–/+	(Ol+Chr), (CGM+Spl +Amp+ Phl+Mgs+Mss+Pn+Cp)

Note: Pressure *P* is estimated with Opx-Grt geobarometer, temperature *T* is estimated with 'Ca-in-Opx' geothermometer,[46] both in accordance with recommendations.[47] The estimates of *P** were obtained with monomineral geobarometer.[48] The geothermobarometric study follows previous procedures.[22,45] The mineral name abbreviations here and throughout the text are according to Whitney and Evans,[49] except for Mss – monosulfide solid solution. Minerals listed in parentheses correspond to the studied polymineral inclusion associations.

Abbreviation: CGM, crichtonite group minerals.

[a]Classified, following Grütter et al.[50]

TABLE 3 Chemical electron microprobe (EMP) analyses of crichtonite group minerals (CGM) included into mantle garnet

Sample grain no.	O-39	M34/01 a	M34/01 b	M34/01 c	M34/01 d	O-173	O-207	UV127/09	O-264	1n11	s21	s291	s328
Oxide contents (wt%)													
SiO_2	0.13	0.17	0.08	0.82	0.05	0.88	0.47	b.d.	0.06	0.04	0.03	b.d.	0.01
TiO_2	68.3	61.3	61.5	60.9	66.6	68.1	63.8	65.8	68.4	60.9	57.4	56.9	57.4
Al_2O_3	2.33	1.68	1.20	1.52	1.39	2.74	3.38	1.23	2.15	1.64	1.27	2.15	1.43
Cr_2O_3	6.58	16.0	14.2	15.0	12.9	2.41	3.86	10.79	7.39	13.1	16.6	17.5	15.4
FeO[a]	10.2	6.69	7.14	7.05	7.99	11.7	9.93	9.10	7.67	8.07	7.34	8.37	8.19
MnO	0.15	0.12	0.15	0.13	0.13	b.d.	b.d.	b.d.	0.09	0.11	0.10	0.10	0.08
MgO	4.18	3.13	3.49	3.57	3.97	5.22	5.17	3.62	5.12	4.29	3.90	3.71	3.48
NiO	0.10	0.04	0.05	0.04	0.07	n.a.	n.a.	n.a.	0.17	0.05	0.03	0.07	0.05
CaO	2.57	2.30	0.99	1.91	2.35	1.26	1.55	0.63	2.65	0.58	0.35	0.44	0.71
SrO	0.08	0.06	0.25	0.32	n.a.	2.58	1.47	1.06	n.a.	0.53	0.22	3.08	0.42
PbO	0.10	0.02	0.05	0.29	n.a.	n.a.	n.a.	n.a.	n.a.	n.a.	n.a.	n.a.	n.a.
BaO	b.d.	b.d.	4.69	0.23	n.a.	n.a.	n.a.	n.a.	n.a.	5.55	6.73	1.06	4.53
Na_2O	0.75	0.51	0.19	0.43	n.a.	n.a.	n.a.	n.a.	n.a.	0.03	b.d.	b.d.	0.04
K_2O	0.12	0.21	0.21	0.40	n.a.	0.63	0.47	0.39	n.a.	0.09	0.03	0.02	0.27
Ce_2O_3	b.d.	0.20	1.56	0.39	n.a.	n.a.	n.a.	n.a.	n.a.	0.06	b.d.	0.75	0.05
La_2O_3	b.d.	b.d.	0.05	0.06	n.a.	n.a.	n.a.	n.a.	n.a.	b.d.	0.04	0.65	b.d.
Y_2O_3	0.01	b.d.	b.d.	0.01	n.a.	n.a.	n.a.	n.a.	n.a.	0.01	0.05	b.d.	b.d.
V_2O_5	b.d.	b.d.	b.d.	b.d.	b.d.	n.a.	n.a.	n.a.	b.d.	0.70	0.66	0.65	0.78
Nb_2O_5	b.d.	b.d.	b.d.	b.d.	b.d.	n.a.	n.a.	n.a.	b.d.	b.d.	0.06	b.d.	b.d.
ZrO_2	2.38	4.82	2.42	4.18	2.59	4.15	4.66	2.36	3.39	1.74	1.66	2.52	4.85
HfO_2	0.02	0.14	0.05	0.21	n.a.	n.a.	n.a.	n.a.	n.a.	0.10	b.d.	b.d.	0.26
UO_2	b.d.	b.d.	b.d.	b.d.	n.a.	n.a.	n.a.	n.a.	n.a.	n.a.	n.a.	n.a.	n.a.
Total	98.0	97.4	98.3	97.4	98.1	99.7	94.8	95.0	97.1	97.5	96.4	97.9	98.0
Mg#	42.2	45.5	46.6	47.4	47.0	44.3	48.1	41.5	54.3	48.7	48.6	44.1	43.1
Cr#	65.4	86.5	88.9	86.9	86.2	37.1	43.3	85.5	69.7	84.2	89.7	84.5	87.8

Note: Letters a, c, and d correspond to oriented CGM inclusions in garnet, and b corresponds to unoriented one. b.d. — below detection limit; n.a. – not analyzed.
[a]Total Fe as FeO. $Mg\# = 100 \times Mg^{2+}/(Mg^{2+} + Fe^{total})$; $Cr\# = 100 \times Cr^{3+}/(Cr^{3+} + Al^{3+})$.

Garnet xenocrysts from the Aldanskaya and Ogonek lamprophyres represent grains 2 to 4 mm in diameter containing primary mineral inclusions (listed in Table 2) that are not associated with cracks. These mineral inclusions in the Aldan samples often have needle- and blade-like morphology with cross-sections of a round or polygonal shape, though subisometric inclusions are commonly recognized as well.[22] Concerning CGM inclusions in the Aldanskaya and Ogonek garnets, they occur essentially as subherdal to euhedral tabular crystals. An inclusion in sample s291 (Ogonek pipe) is polymineralic and comprises CGM, Cr-spinel, amphibole, phlogopite, magnesite, and a sulfide speck, the latter being composed of pentlandite—monosulfide solid solution tight intergrowths surrounded by a chalcopyrite rim (Figure 2). The whole inclusion is roughly isometric (~100 × 150 μm) and petrographically is not oriented inside the garnet matrix.

Garnets from the examined xenoliths and xenocrysts contain CGM forming whether only oriented inclusions ($n = 13$), or only unoriented ($n = 3$) ones, or both ($n = 2$). In the morphologically oriented intergrowths, CGM make up the inclusions commonly occurring as a net of μm-sized needles, rods, lamellae, and blades together with other minerals listed above. Needle-like CGM are usually regularly spaced and morphologically oriented in a garnet parallel to <111>. These are no more than several micrometers thick, but length may be several tens of micrometers (Figure 1a–f). Blade or rod-like CGM are also oriented in most cases but are occasionally randomly

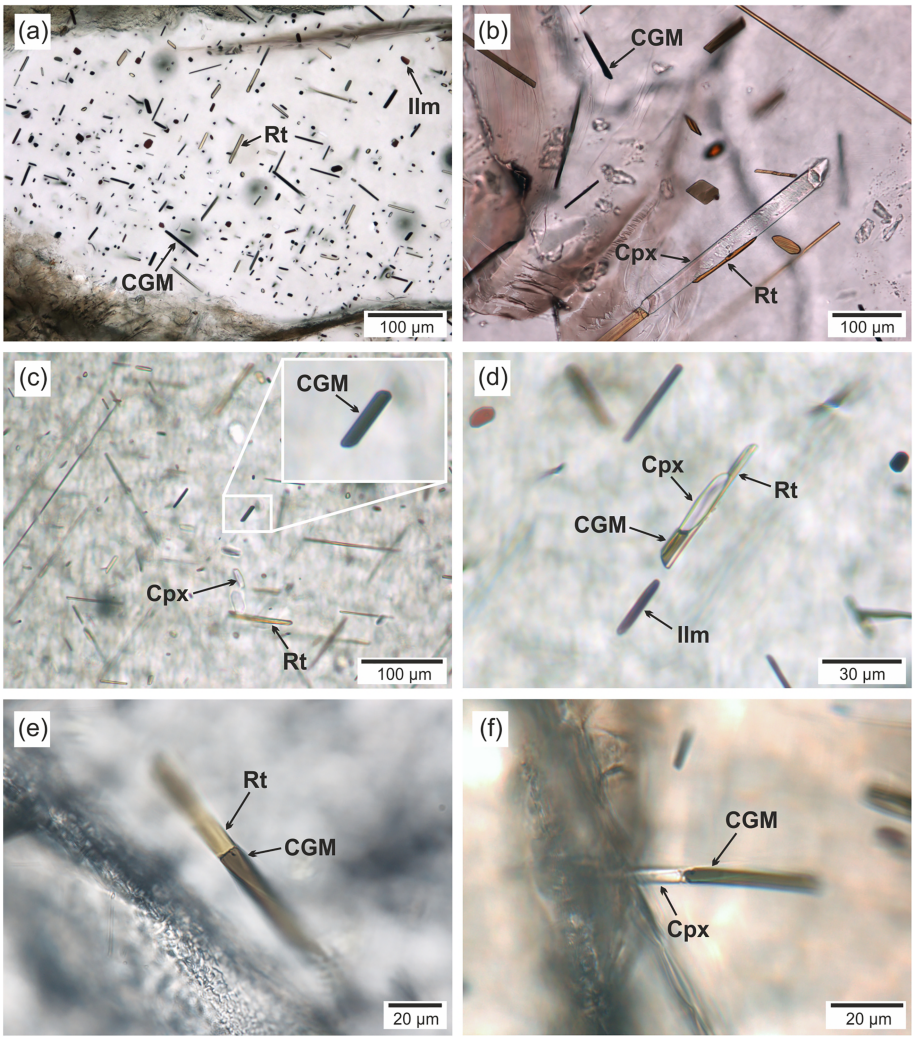

FIGURE 1 Crichtonite group minerals composing inclusions with shape-preferred orientation in mantle xenolith garnets. (a) general overview of monomineral oriented inclusions (O-173, Obnazhennaya pipe); (b) CGM needle inclusions and Cpx + Rt intergrown lamellae (M34/01, Mir pipe); (c) CGM monomineral oriented inclusion together with Rt and Cpx precipitates (O-207, Obnazhennaya pipe); (d) CGM intergrown with Cpx and Rt (O-207, Obnazhennaya pipe); (e) polymineral lamella of CGM + Rt (O-39, Obnazhennaya pipe); (f) polymineral lamella of Cpx + CGM (O-173, Obnazhennaya pipe). Optical images are made in a plane polarized light. CGM, crichtonite group minerals

distributed. Commonly occurring as single crystals, CGM may also coexist with other minerals (e.g., acicular rutile and clinopyroxene) in elongated intergrowths (Figure 1e–f).

The inclusions of CGM of more than 10 μm thick are usually opaque, black in color, and with sub-metallic luster, similar to other members of the crichtonite group met in mantle environment.[37] Thin needles/rods/lamellae and edges of thicker inclusions are transparent or translucent, with color from brownish green to dark grayish green for low-Cr varieties, and brownish red for Cr-rich ones.

4 | MINERAL CHEMISTRY

4.1 | Host garnet

Major-element compositions of garnet from the studied xenoliths and xenocrysts fall in a range of typical mantle pyrope-rich chemistries with proportions of $Prp_{68.5-76.9}Alm_{9.3-18.7}$

$Uv_{1.0-7.7}Grs_{2.9-9.3}$ for the Obnazhennaya, $Prp_{66.0-69.7}Alm_{15.4-17.6}Uv_{4.2-13.3}Grs_{0.0-5.6}$ for the Udachnaya and Mir xenoliths, together with $Prp_{65.5-67.8}Alm_{16.0-16.8}Uv_{10.0-12.7}Grs_{0.0}$ for the Aldanskaya and Ogonek xenocrysts, whereas other components (Knr, Scl-Al, Mrt, NaTi Grt, Mrt-Mg, Maj, Sps, Adr, and Skg) comprise no more than 1.5–5.1 mol.% in proportion (Table S2). The end-members were calculated and named in accordance with Locock.[51] Compositions and parageneses of garnet grains in the studied xenoliths are unambiguously determined by the whole-rock chemistry, whereas the paragenetic derivation of the garnet xenocrysts from the Aldan lamprophyres has been determined as 'lherzolitic (G9)' (Table 3, Grütter et al[50]). The contents of chromium (Cr_2O_3 0.34–5.42 wt%), calcium (CaO 3.68–5.96 wt%), and titanium (TiO_2 0.06–0.31 wt%) as well as magnesian number ($Mg\#\{=100\times Mg^{2+}/(Mg^{2+}+Fe^{total})\}$76.9–86.5) differ significantly. Chromium number $Cr\# = 100\times Cr^{3+}/$

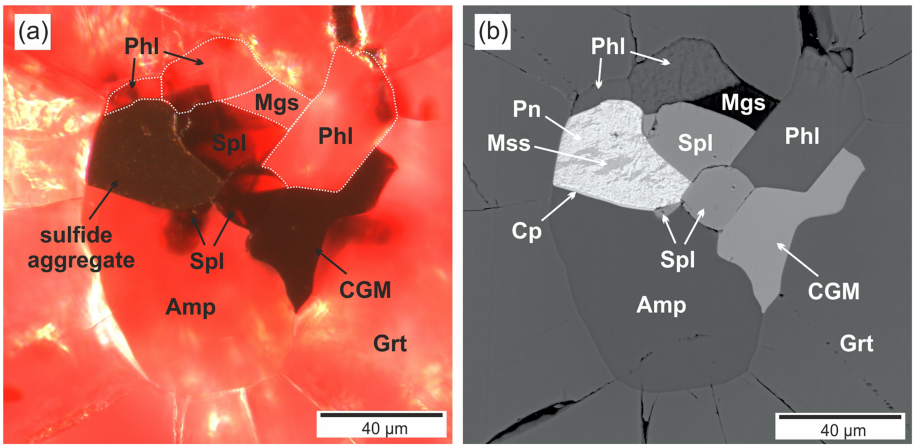

FIGURE 2 Polymineral inclusion in a garnet xenocryst from the Ogonek lamprophyre (sample s291). (a) Optical microscope plane polarized light image. (b) Back-scattered electron (BSE) image. Sulfide aggregate is composed of tight intergrowths of monosulfide solid solution and pentlandite rimmed by chalcopyrite. CGM, crichtonite group minerals

$(Cr^{3+} + Al^{3+})$ ranges from 1.0 to 15.1, with the highest value for the Aldanskaya garnet (Sample s21), whereas the lowest figures are typical of the Obnazhennaya garnet grains (Sample O-207). The TiO_2 variations within individual crystals are minor, mostly less than ±0.03 wt%. The difference in Cr_2O_3 content with variation larger than ±0.08 wt% was found only in a few samples; the most pronounced one from core (2.73) to rim (2.30) is observed in Sample O-571. Other element variations are within analytical accuracy (Table S2). Thus, garnet host grains widely show no core-rim zoning. The contents of Na_2O are usually less than 0.10 wt%.

4.2 | Crichtonite group minerals

The composition of the CGM is various among different garnet grains from a set of the studied samples. Nevertheless, it is close to uniform for species with the same morphology within individual host garnet grains; in these grains, variation of oxide contents falls into the analytical accuracy range (Table 2).

The A-site position is occupied mainly by Ca, Na, Sr, K, Ba, Ce, and La cations. The B-site is dominated by Zr or Fe, and the C-site cations include Ti, Cr, and Fe with noticeable Al, the Mg with fewer amounts of Fe and Mn fill in the T-site (Table 4). The compositions of the studied CGM vary in TiO_2 (ranging from 56.9 to 68.4 wt %) and Cr_2O_3 (ranging from 2.41 to 17.5 wt%). As Ti and Cr cations occupy the same C-position, the TiO_2 and Cr_2O_3 contents are in roughly negative correlation with each other. The values of Cr# vary significantly from sample to sample (37.1 to 88.9). Similar to previous observations,[24,37,39] the Cr_2O_3 content in CGM is in strong positive linear relationships with that of the host garnet ($R = +0.97$ for both core and rim garnet compositions, $n = 13$). Weaker interdependence in between Al_2O_3 content in garnet and CGM ($R = +0.83$ for both garnet cores and rims) as well as in between Mg# of garnet and ZrO_2 content of CGM ($R = -0.72$ for garnet cores and −0.74 for garnet rims) has been noticed.

5 | RAMAN SPECTROSCOPIC RESULTS

5.1 | Experimental and theoretical basis

To study the mineralogy of inclusions composing a morphologically oriented network in garnets, high precision methods are necessary. Small size of mineral grains restricts the application of EMP and SEM methods for the routine mineral identification. In that case, Raman spectroscopy allows identifying small-sized minerals, including those unexposed on the host mineral surface. Our first measurements were devoted to recognize CGM and distinguish them from other mineral species usually composing oriented needles in mantle garnets. For this purpose, those needles that had been preliminary studied with EMP and SEM (examples are shown in figure 6a,b in Alifirova et al[40]) and had shown compositions closest to CGM (in a calculation to mineral formula) were taken. Samples O-207, O-173, and UV127/09 were employed as inner standards. These standards were studied by an optical microscope to recognize the typical features of CGM, like their color, transparency, and morphology (Figure 1).

5.2 | Factor-group analyses and band assignment

The CGM have a crystal structure with rhombohedral symmetry that belongs to the R−3 space group (No. 148), the point symmetry C_{3i} (= −3). The CGM structure is based on the closest-packed anion lattice having a nine-

TABLE 4 Formula representation for the studied crichtonite group minerals (CGM)

Sample grain no.	O-39	M34/01 a	M34/01 b	M34/01 c	M34/01 d	O-173	O-207	UV127/09	O-264	1n11	s21	s291	s328
Formula assignments to 38O													
A (ideally 1 apfu)													
Na	0.408	0.284	0.105	0.237	0.000	0.000	0.000	0.000	0.000	0.017	0.000	0.000	0.023
K	0.041	0.077	0.079	0.147	0.000	0.224	0.175	0.143	0.000	0.034	0.012	0.008	0.102
Ba	0.000	0.000	0.539	0.026	0.000	0.000	0.000	0.000	0.000	0.640	0.794	0.123	0.526
La	0.000	0.000	0.006	0.007	0.000	0.000	0.000	0.000	0.000	0.000	0.004	0.071	0.000
Ce	0.000	0.021	0.167	0.041	0.000	0.000	0.000	0.000	0.000	0.006	0.000	0.082	0.005
Sr	0.013	0.010	0.043	0.053	0.000	0.420	0.249	0.180	0.000	0.090	0.038	0.530	0.072
Pb	0.008	0.001	0.004	0.022	0.000	0.000	0.000	0.000	0.000	0.000	0.000	0.000	0.000
$Ca^{XII}A$	0.530	0.607	0.056	0.467	0.704	0.355	0.576	0.676	0.794	0.212	0.152	0.186	0.272
A subtotal	1.000	1.000	1.000	1.000	0.704	1.000	1.000	1.000	0.794	1.000	1.000	1.000	1.000
B (ideally 1 apfu)													
Zr	0.324	0.673	0.346	0.586	0.354	0.568	0.664	0.336	0.462	0.250	0.244	0.365	0.701
Y	0.001	0.001	0.000	0.002	0.000	0.000	0.000	0.000	0.000	0.000	0.000	0.000	0.000
Hf	0.002	0.013	0.005	0.020	0.000	0.000	0.000	0.000	0.000	0.010	0.000	0.000	0.026
$Fe^{VI}B$	0.787	0.338	0.613	0.318	0.892	0.580	0.513	1.153	0.549	1.120	1.166	1.450	0.647
$Ca^{VI}B$	0.240	0.097	0.255	0.120	0.000	0.024	0.000	0.000	0.000	0.000	0.000	0.000	0.000
B subtotal	1.355	1.122	1.219	1.045	1.245	1.172	1.178	1.490	1.011	1.380	1.410	1.815	1.373
T (ideally 2 apfu)													
Mg	1.743	1.333	1.528	1.527	1.655	2.188	2.255	1.573	2.132	1.882	1.751	1.643	1.537
Mn	0.035	0.030	0.038	0.031	0.031	0.000	0.000	0.000	0.020	0.027	0.026	0.025	0.020
$Fe^{IV}T$	0.221	0.637	0.434	0.441	0.314	0.000	0.000	0.427	0.000	0.091	0.224	0.332	0.443
T subtotal	2.000	2.000	2.000	2.000	2.000	2.188	2.255	2.000	2.152	2.000	2.000	2.000	2.000
C (ideally 18 apfu)													
Ti	14.374	13.188	13.576	13.140	14.014	14.390	14.028	14.449	14.375	13.473	13.004	12.705	12.791
Cr	1.455	3.614	3.294	3.404	2.849	0.536	0.892	2.489	1.633	3.035	3.940	4.102	3.607
Al	0.769	0.565	0.413	0.513	0.457	0.907	1.165	0.422	0.709	0.569	0.451	0.753	0.499
Nb	0.000	0.000	0.000	0.000	0.003	0.000	0.000	0.000	0.000	0.000	0.008	0.000	0.000
V	0.000	0.000	0.000	0.000	0.000	0.000	0.000	0.000	0.000	0.136	0.131	0.128	0.153
Ni	0.021	0.009	0.012	0.010	0.016	0.000	0.000	0.000	0.037	0.012	0.007	0.017	0.012

TABLE 4 (Continued)

Sample grain no.	O-39	M34/01 a	M34/01 b	M34/01 c	M34/01 d	O-173	O-207	UV127/09	O-264	1n11	s21	s291	s328
$Fe^{VI}C$	1.381	0.623	0.705	0.933	0.662	2.167	1.915	0.639	1.246	0.775	0.458	0.296	0.939
C subtotal	18.000	18.000	18.000	18.000	18.000	18.000	18.000	18.000	18.000	18.000	18.000	18.000	18.000
Sum													
A, B, T, C	22.355	22.122	22.219	22.045	21.949	22.360	22.432	22.490	21.957	22.380	22.410	22.815	22.373

Note: The data for the calculations are presented in Table 2.

layer stacking sequence (hhc...) in which the ^{XII}A (M0) cation occupies an anion site. The other cations are ordered into 19 octahedral, that is, ^{VI}B and ^{VI}C (M1, M3, M4, and M5), and 2 tetrahedral, that is, ^{IV}T (M2), sites per a primitive unit cell. The M1 and M3 octahedra form one layer, whereas the M0, M2, M4, and M5 polyhedra form a double layer.[3,7,12,15,16]

Because most of the studied CGM species from mantle garnets are considered as chemical analogues of loveringite, the latter was examined in terms of factor-group analysis using Bilbao Crystallographic Server.[52] Crystal structure data for both natural samples[15] and synthetic (Sample 9b[53]) counterparts have been taken into account.

According to the structural data, the parameters of the primitive cell for natural loveringite are $a' = b' = c' =$ 9.117 Å and $\alpha = \beta = \gamma$ =69.070°.[15] The generalized formula, following our recalculation, is $[Ca, LREE, Pb]^{A}_{1.000}\,{}^{B}_{1.000}[Zr, Fe, Ca, (Y, Th, U, Hf)]^{B}_{1.375}{}^{C}_{1.375}[Ti, Fe, Cr, Al, V, Nb, Ni]^{C}_{18.000}{}^{T}_{18.000}\,[Mg, Fe, Mn]^{T}_{2.000}O_{38}$. One hundred and two Raman active vibrational modes are allowable, following the symmetries: $\Gamma_{Raman} = 51A_g + 51E_g$, where each E_g mode is double degenerated $E_g = E_g{}^1 + E_g^2$. The only contributors of the Raman spectral features of this oxide are to be ionic groups of cations from octahedral interstices (all having 18*f* Wyckoff position), the major of which is $Ti^{4+}O_6$.

Regarding the synthetic sample,[53] the parameters of the primitive cell are $a' = b' = 10.42$ Å, $c' = 20.9413$ Å, and $\alpha = \beta$ =90° , γ =120°. The generalized formula is $Ca^{A}_{1.000}[Ca, Mn]^{B}_{1.000}[Mn, Ti^{3+}, Ti^{4+}]^{C}_{18.000}Mn^{T}_{2.000}O_{38}$. For this loveringite, 64 Raman active modes are assigned: $\Gamma_{Raman} = 32A_g + 32E_g$. Ionic groups with cations of 18*f* and 6*c* Wyckoff position represent a major contributor to the Raman spectral features. The cationic groups make up octahedral and tetrahedral interstices and, considering the synthetic sample,[53] are $Ti^{4+}O_6$ and $Mn^{2+}O_4$.

Both cases clearly show that the cations occupying the 12-coordinated M0 and the eightfold M1 positions do not contribute to the Raman spectral features. The latter was approved by our Raman experimental study. Even the significant variability of the A- and B-site occupancies in the investigated mantle samples from different localities does not introduce significant differences in the Raman spectra features (Figures 3 and 4, Table 4). Nonetheless, the factor-group analysis evidences the difference in Raman spectra to depend on a cation distribution between the M2–M5 polyhedra. Noticeable proportion of Fe in the Mg-rich tetrahedra, and substitutions of Ti by Cr, Fe, and Al in the C-site octahedra in our samples, is responsible for the slight variations of the Raman band disposition, and this difference is even more obvious if

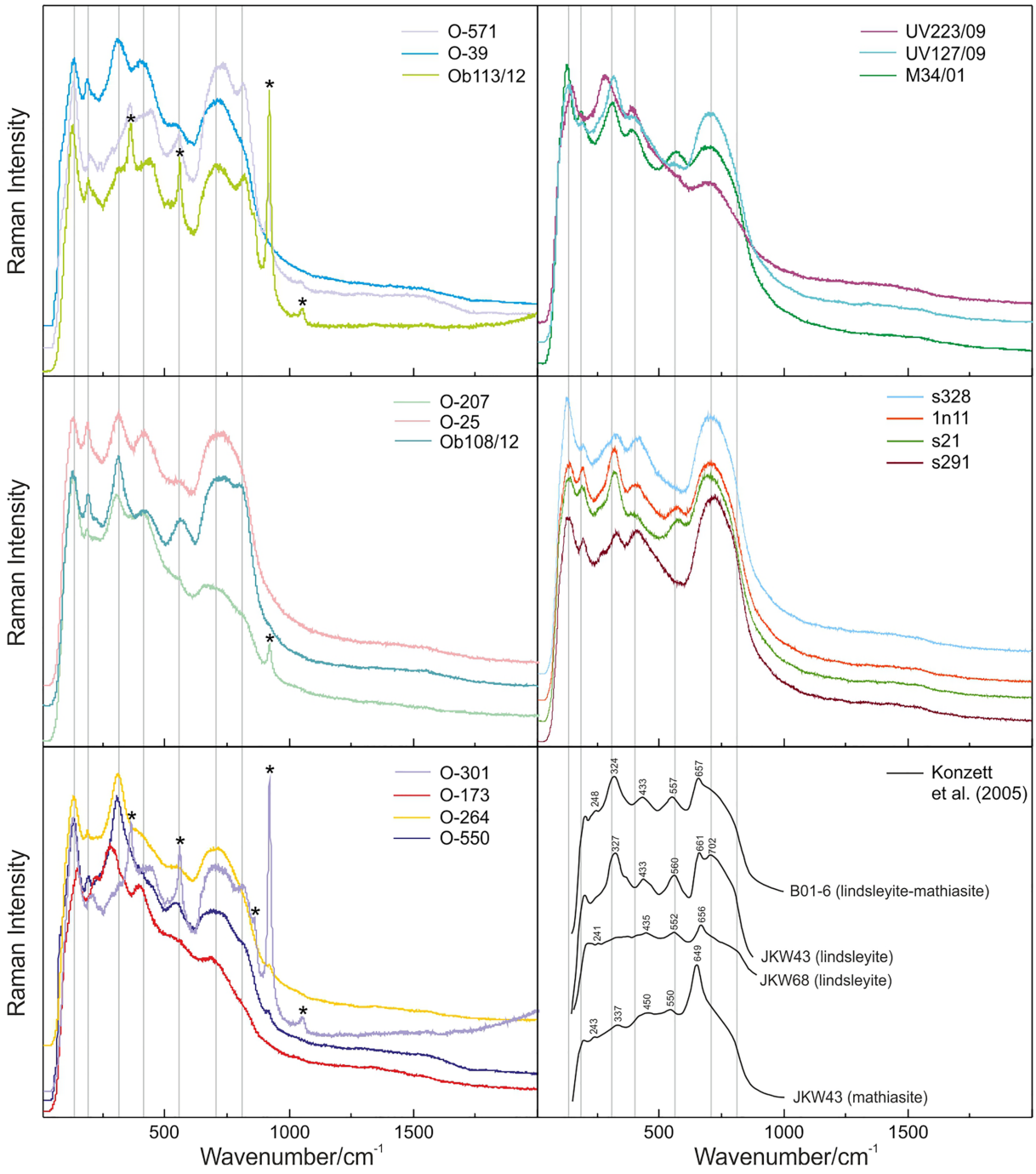

FIGURE 3 Raman spectra of the crichtonite group minerals included into the garnet from the investigated mantle samples. Sharp peaks from the host garnet are indicated by stars (*)

comparing our Raman data with those for synthetic samples (Figure 3, Konzett et al[18]).

5.3 | General Raman features of CGM

The spectra of CGM cover a range of wavenumbers from low ones to 1,000 cm^{-1}, with the most intensive modes allocated within a region of 100–850 cm^{-1}. The latter is consistent with the CGM chemistry, as they are composed of heavy elements, mostly metals, occupying oxygen-framed positions and held in the crystal structure by ionic bonds.

Similar to many other Fe-Ti-Cr-oxides like ilmenite, or those of spinel- and magnetoplumbite-groups (e.g., Konzett et al[18] and Wang et al[54]), CGM produce lower Raman signals than oxyanionic minerals and Ti and Al oxides and represent weaker Raman scatters. This

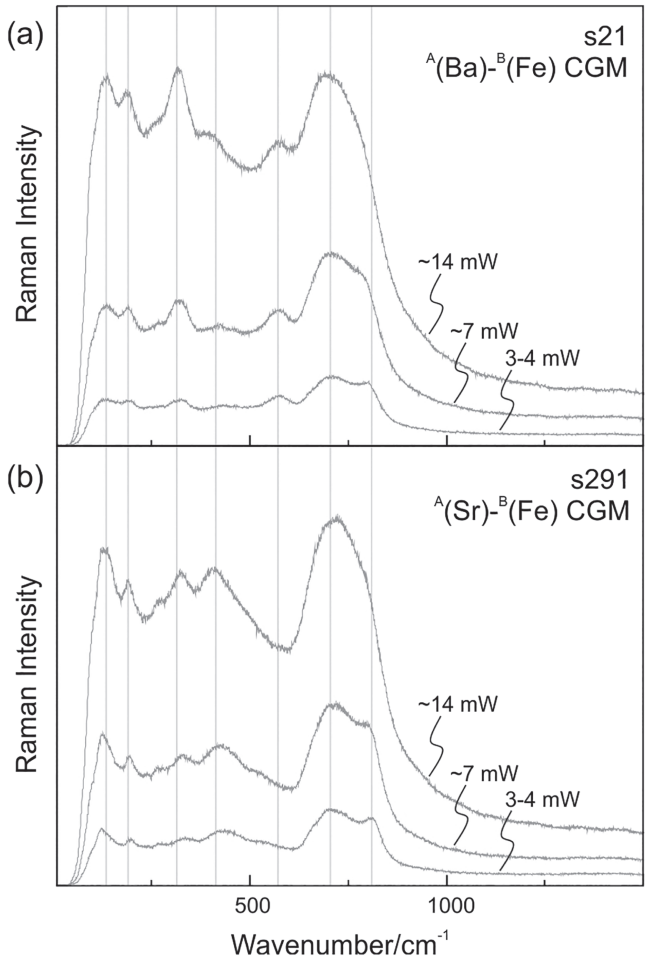

FIGURE 4 Plot showing the dependency between laser beam power and intensity of modes in the Raman spectra of CGM from Aldanskaya and Ogonek garnet xenocrysts. CGM, crichtonite group minerals

difference can be partially attributed to dark colors of CGM in thick and dense grains, limiting the penetration depth of the excitation laser beam (visible wavelength) and produced Raman radiation. It should be noted that when measuring dark thick granular inclusions from the studied collection (e.g., Aldanskaya samples), it was found that the intensity of the strongest peaks was several times lower than that of thin lamellar inclusions and inclusion thin edges.

A small difference of intensities in the CGM Raman spectra is explained by that bond strength difference between different types of polyhedra (e.g., TiO_6 octahedra and FeO_4 tetrahedra) is less pronounced, and overall degree of covalency is much lower than that in silicate, phosphate, carbonate, and sulfate compounds. Moreover, polyhedra in the CGM structure are more or less rigid that is supported by their bulk modulus. Upon watching a number of Raman-active modes in CGM, the question arises why not all the modes are pronounced in the measured spectra. First of all, the modes are likely overlapped, and second, only major contributing modes can be recognized due to the aforementioned reasons (Table 5, Figure 5). The cation substitutions can cause a change in spectral features (Figure 3, Section 5.2), and major modes have different intensities (Figure 4).

The position and shape of the strongest peaks of CGM in the regions of 100–200, 300–450, 700–850 cm^{-1} (A_g translation, bending, and stretching modes, respectively) are the most useful for discriminating CGM. Minor peaks (E_g symmetry) in the region of 100–900 cm^{-1} also assist in the recognition, especially when delineating characteristic features of various CGM species. These spectral properties are valuable to investigate variability amid Fe-Cr-Ti oxide solid solution series in natural samples.

5.4 | Raman features of the studied CGM

Due to the lack of the loveringite Raman spectra in the database, we have compared the collected spectra with those of other mineral species that belong to the crichtonite group, in particular synthesized LIMA minerals,[18] dessauite-(Y) from La Beaume, Oulx, Susa Valley, Piedmont, Italy, and gramaccioliite-(Y) from the Sambuco, Stura Valley, Cuneo Province, Italy,[9] as well as crichtonite from the Presidente Kubitschek, Minas Gerias, Brazil (RRUFF ID 090006; Lafuente et al[25]), and davidite-(La).[8] The particular CGM species for which we report the Raman data are indicated in Table 1.

The comparison between the Raman spectra recorded from 10 to 2,000 cm^{-1} of the studied crystals and those of synthetic LIMA minerals[18] is shown in Figure 3. The close matching between the collected spectra is observed. The main Raman bands of CGM are located in the region between 100 and 200, 300 and 450, 650 and 850 cm^{-1}; the strongest ones are at 130, 300–310, 410–440, 710–720, and 810–820 cm^{-1}. Other weaker, broad, and shoulder-like bands are visible at 190, 208–215, 457–467, 538–556, 365 and 660 cm^{-1} (Figure 5).

The investigation of the O–H bond bending and stretching region (3,200–3,800 cm^{-1}) showed no Raman-active modes, either at commonly used 14 mW or at lower laser beam power values. Thus, this region is not depicted in the Raman spectra plots (Figures 3, 4, and 5).

It was found that high energy of the laser produces either strong fluorescence or destruction of the mineral, making Raman signal much weaker (even 'flat') or noisy, and in both cases, no detectable Raman spectra can be collected. The destruction of LIMA minerals under the laser irradiation was described previously.[18] In the present study, CGM with prevailing Ba and Sr in the A-site

TABLE 5 Gaussian function peak fitting results for the Raman spectrum of CGM from Grt-lherzolite garnet O-39

Fityk baseline correction			CrystalSleuth baseline correction		
X Position	**HWHM**	**Amplitude**	**X position**	**HWHM**	**Amplitude**
79.7	12.5	2097.0	75.0	6.5	1680.4
			85.7	8.0	714.2
			91.7	13.0	1231.0
108.2	67.7	6223.6	104.8	6.9	330.2
			126.6	27.7	2682.9
188.1	12.7	677.9	186.7	10.2	733.8
			208.0	11.9	228.9
215.6	34.6	1860.5	215.4	2.1	39.5
			238.5	3.4	101.1
310.8	66.2	5202.0	300.5	20.1	749.9
			324.1	0.0	87.2
			328.4	17.4	327.6
398.2	33.5	2233.7	418.7	26.0	481.6
435.2	30.6	1519.3	440.1	12.1	79.0
467.7	38.9	1887.0	457.2	10.7	182.4
538.4	54.2	2251.1	555.8	25.5	401.0
660.0	16.0	1647.0	661.2	17.2	330.7
717.9	113.2	3877.2	712.4	31.4	261.5
823.1	28.1	491.5	823.7	19.0	300.4
951.9	124.5	470.4	929.1	17.8	130.5
			981.1	37.8	66.1
1159.0	53.8	60.6			

Abbreviation: HWHM, half width at half maximum.

(for example, samples from the Aldanskaya dike and Ogonek diatreme) showed the same behavior. The CGM rich in Sr, Ce, and La from the Obnazhennaya kimberlite are noticed to be affected by a laser as well. Nevertheless, all these species become destructed under laser only when exposed onto the surface, whereas being inside the host garnet, CGM do not show observable destruction features. It should be noted that relative peak intensity in the Raman spectra for the destructed minerals was lower than that for the nondestructed ones, what highlights in turn that the lower laser beam power is desirable but not mandatory to analyze CGM.

The dependence of the Raman spectrum appearance on the laser beam power is presented in Figure 4. It can be noticed there that the Raman band around 820 cm^{-1} is more pronounced at the lower laser beam power, whereas at the higher power, this band has a shoulder shape. Alike feature can be seen in the spectra of samples O-173 and O-207 (Figure 3), where the band at 820 cm^{-1} is smoothed to a shoulder-shape. The CGM in these samples showed intense laser-induced destruction. The occurrence of the shoulder-shaped band in a direction to the higher frequency shift values in fact may be taken as an indicator that the examined crichtonite-group mineral was damaged under the laser beam. The CGM that are close in composition to loveringite species (A-site is occupied mostly by Ca) show low or nearly indistinguishable destruction under the laser irradiation when being either on or under host garnet surface.

We noticed the translucent needles or thin edges of CGM to give better Raman spectra (Figure 1), whereas large intransparent grains and thick plates often provide no enough or much lower signal. Some of the CGM showed luminescence effect on the Raman spectra when using 633-nm excitation wavelength laser, whereas with 488- and 532-nm lasers, this effect appears to be lower. It means that certain luminescence centers become excited under red rather than blue and green laser. As a rule, the CGM studied with 633-nm excitation wavelength laser showed lower intensity Raman spectra, compared with those taken with shorter-wavelength illumination (488- and 532-nm lasers). In case of using a filter-decreased

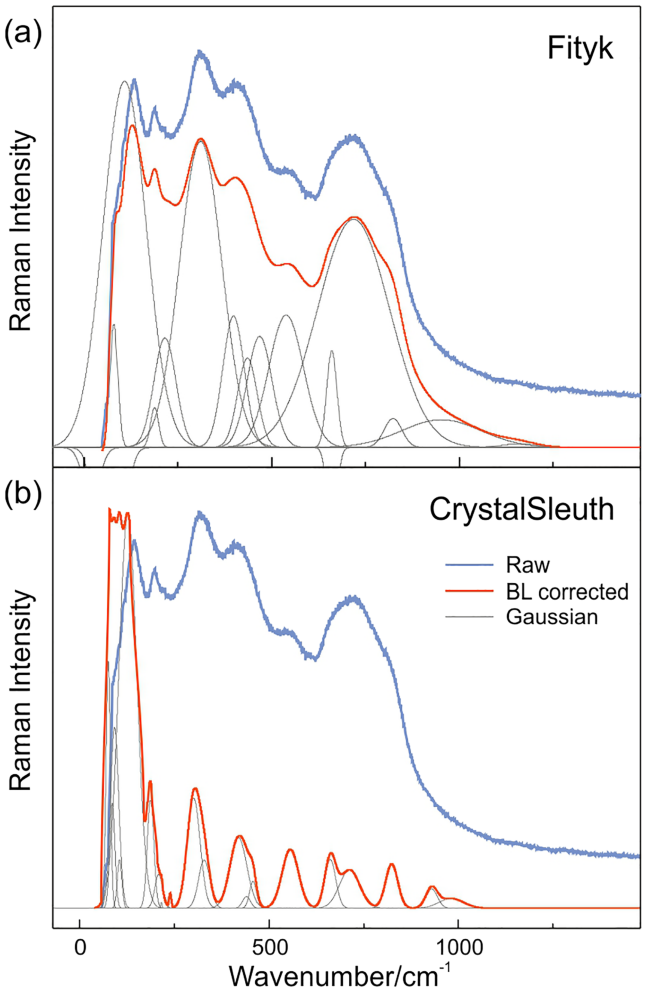

FIGURE 5 Peak fitting modeling for the Raman spectrum of an oriented CGM inclusion in garnet, Sample O-39. The raw spectrum was baseline (BL) corrected with Fityk[55] (a) and CrystalSleuth[56] (b) software

laser beam power at 532 nm and a normal (unfiltered) laser beam power at 633-nm illumination, when Raman signal from both green and red excitation is low, the CGM spectra are relatively noisier if induced by a red laser. These effects can be explained by the inverse dependence of the Raman scattering intensity, detector sensitivity, and spatial resolution (and, thus, a noise level) from illumination wavelength.

6 | DISCUSSION

6.1 | Dependence of the CGM Raman features on their chemistry

According to the theoretical constraints, there should be 64 Raman-active vibrational modes in the Raman spectrum of synthesized 'loveringite'.[53] There is still an uncertainty whether the spectrum of natural loveringite contains the same number of modes. The loveringite Raman spectrum has been found neither in publications nor in the RRUFF database.[25] The latest structure refinement data of the natural loveringite were reported following a simpler formula $AB_{21}O_{38}$,[15] and the number of Raman-active modes for this oxide accounts 102. Current data for the oxide compounds of the crichtonite group require present structural data for natural loveringite and its analogues to be up-to-date. In particular, the distribution of cations between positions can be unclear, taking into account that Ca in loveringites can enter both the M0 and M1 positions. Nevertheless, the latter is unlikely to significantly affect the Raman features, as the M0 and M1 site occupancies hardly contribute to the Raman spectra.

The Raman band assignment can be complicated as large amount of Raman-active modes is disposed within comparably narrow frequency shift region. These modes are produced by vibrations of cationic groups in which metal-oxygen bonds are characterized by moderate covalency degree, similar to other Fe-Ti-Cr oxides.[54] The moderately ionic character of the chemical bonds regulates shape of the Raman bands which, correspondingly, are relatively lower in their intensity and have larger FWHM values, compared with the Raman bands assigned to vibrations of strongly covalent bonds. Regarding the CGM Raman spectra, broad and smooth bands are observed around 310, 430, 550, 660, 720, and 820 cm^{-1} (Figure 3). Due to the wide and low-amplitude features of the CGM Raman bands, their large amount may appear merged in the Raman spectra (Figure 5, Table 5). In that case, deconvolution of the spectra may become a matter of subjective view. An alternative explanation of why the Raman bands may be merged or broadened is as follows. When comparing the Raman spectra of the CGM presented in this study and in Konzett et al,[18] the difference in FWHM of the CGM Raman bands can be noticed (Figure 3). Those in our natural samples, whose chemistry is an intermediary of a substitutional solid solution, are all wider and comparatively lower-intensive than the Raman bands of the pure, synthesized compounds. Similar difference between Raman spectra of end-members and their mixtures is observed in other minerals, for example, in garnets.[57]

Despite the fact that the exact recognition of all possible Raman modes is difficult, the recorded CGM Raman spectra are clearly distinguished from those of the other oxides (like ilmenite or those belonging to the spinel- and magnetoplumbite-groups; Konzett et al[18] and Wang et al[54]) and, to a lesser extent, among individual species within the group (Bittarello et al[9] and Frost and

Reddy[8]), and carry a number of diagnostic features that are applicable to the accurate identification of CGM. Obtained results demonstrate the Raman spectra of CGM to contrast with those of aforementioned optically and chemically similar compounds due to difference in crystal structure and chemical bond vibrations. A slight variation in the Raman peaks position of the CGM spectra from this and previous studies is explained by the wide diversity in the CGM solid solution series (Figures 3 and 5, Tables 1 and 3), and it is strongly dependent on which cations predominate in the C and T positions.

Our study includes the Raman data for loveringite, lindsleyite, and their chemical analogues (Table 1). The latter might represent new mineral species (e.g., Samples O-173, O-39, s328, s21, 1n11, and s291). Alike CGM were described in the Khibiny alkaline complex,[23] as well as inclusions in garnet xenocrysts from the Internatsionalnaya kimberlite[24,39] and Garnet Ridge ultramafic diatreme, Colorado Plateau.[37] Some of them are akin to Na-Sr-rare earth element (REE) titanates of the crichtonite group that were suggested as distinct mineral species.[23] It is noteworthy that in the CGM from the Khibiny carbonatites, Fe prevails over Zr and the portion of Ca is high as well,[23] whereas Cr contents are low compared with the Siberian CGM. Regarding the CGM from the Internatsionalnaya kimberlite,[24] one of the species (INT-15) chemically equivalent to the Ogonek sample studied here (s291) was examined by a single-crystal X-ray structure analysis proving a match of diffraction patterns by that of CGM. In our samples, there are species rich in Sr, Ba, or Na (along with Ca) in the A-site, whereas in the B site, the Zr or Fe prevails over other cations, and Cr is an essential (though not prevailing) component of the C site. Hence, our chemistry data extend the dataset for CGM occurring in natural environments. They also obviously demonstrate that a review of structural refinement data for mantle CGM is on demand to expand views on isomorphic series of CGM and improve their nomenclature.

6.2 | Specific spectral diagnostics of CGM: luminescence and metamictization

Our Raman study revealed some CGM spectra to be interfered by luminescence. Luminescence has been considered as one of the diagnostic features of CGM (e.g., Bittarello et al[9]). The effect of luminescence may hide minor Raman bands or make major ones look broader and lower intense, though it can be decreased by using a lower laser beam power. Nevertheless, it can not be fully avoided in case of species enriched by elements which are luminescence centers, that is, lanthanides (e.g., La, Ce, and Pr), actinides (U), and transition metals (e.g., Y and Cr). As it was shown, for example, for the other REE-enriched accessory minerals,[58] the emission of listed elements and its intensity are controlled by laser illumination wavelength and by energy-dependent nature of different luminescence centers to excite. In this case, to record the Raman spectra, one may also need to select the excitation wavelength based on the chemical composition of CGM.

Furthermore, the effect of metamictization of minerals may cause the same influence on the Raman spectra because the crystal structure can become partially destroyed and/or amorphous. We compared our data with the Raman spectra of cleusonite, dessauite-(Y), and gramaccioliite-(Y),[9] and the Raman spectra acquired in this study look similar to those of uranium-bearing CGM varieties. It is accepted that the species of the crichtonite group such as cleusonite,[4] davidite-(La), and davidite-(Ce),[7,8] dessauite-(Y),[2] loveringite,[15] mapiquiroite,[12] and mianningite[14] demonstrate partially metamict features. The partially metamict crystals also show poor X-ray diffraction patterns[14] that appears to be a widespread phenomenon among about a half of CGM species.[12,13] The radiation damage affects a 'quality' of the Raman spectra.[9] It has been shown previously that heating up to 1,000° C, annealing for several hours and final recrystallization causes rearrangement of the CGM structure, which makes it possible to obtain single-crystal diffraction patterns.[14] This approach, in turn, is supposed to help in acquiring Raman measurements for radiation-damaged CGM.

With that in mind, however, the widening of several Raman bands is unlikely to result from the partial occupation of the M0 and M1 sites by lanthanides, actinides, and fission products. Although it may rather reflect the change of valence, further valence balance, and/or change of coordination number, which thus leads to re-partitioning of cations between sites, like it happens in case of U^{4+} and U^{6+}. A decay of some large-ion elements may occur only in the M0-site,[35] nevertheless, liberated electrons might be taken up by transition metals with variable oxidation states such as Ti^{4+}, Cr^{3+}, Fe^{3+}, and V^{5+}, and extra vibrations may occur and merge in Raman spectra, as these elements occupy M-sites that are active for Raman scattering. At the same time, the decay of other elements (e.g., ^{90}Sr to Zr) may involve the diffusion of cations from M0 to M1 or other M sites.[35] If so, the radiation damage effect is owing to be observed in Raman spectra because it may introduce variability to the Raman spectra shape.

An excess of cations (including radionuclides and fission products) in the sites of the CGM structure is related to the capacity of the crichtonite structure type to hold a

significant amount of vacancies compensating charge,[18] and it is usually observed in natural CGM (e.g. Barkov et al[23]). Radioactive damage metamict features reflected in the Raman spectra of CGM are an outstanding example of how the physical and chemical properties may be changed due to alpha-decay of elements, especially U and Th. Metamict features may serve as diagnostic ones while searching for crichtonite minerals. Moreover, metamictization may be an explanation, why some CGM crystals yield poor and noisy Raman spectra. The metamictization effect along with a complex composition of CGM containing transitional metals may elucidate also, why their chemical composition should be sensitive to the environment oxidation state.[53]

6.3 | Composition of CGM and crystal-chemical implications

The CGM chemical composition acquired by means of EMP analysis commonly has a total below 99 wt%. It takes place even if the EMP routine includes measurements of 22 elements, and SiO_2 is added into a set of elements to control the analyses quality and contamination by the host mineral. Formula calculations show that the total of elements with large ion radius occupying the A site in the CGM crystal structure may exceed unity if considering all Ca to enter it. It has been shown previously that Ca is able to enter the B site. In that case, the excess of cations is spread homogeneously between the cation positions. The sum of elements from all the A, B, C, and T sites per 38 oxygen either is close to or exceeds 22. Alike features have been noticed earlier for the CGM from the Khibiny.[23] Regarding chromium-rich CGM, the excess of cations per formula is systematically higher, and for CGM containing >15.5 wt% of Cr_2O_3 like those from the samples GRPy-40 and GRPy-43 (Garnet Ridge ultramafic diatreme, Colorado plateau[37]) and samples INT15 and INT66 (Internatsionalnaya kimberlite pipe, Siberian craton[24]), the cation sum is equal to 22.7 to 23.2. The higher proportion of cations per formula may result from keeping charge balance, and it was noted that the total electroneutrality of compounds is commonly kept. The studied xenolithic CGM ($n = 9$) have a mean cation charge of 76.13 (σ 0.56). For example, the Khibiny CGM[23] ($n = 1408$) have the cation charge equal to 76.08 on average.

Our results of analysis indicate that bond vibrations within the «water» region do not occur in the Raman spectra. The factor group analyses partially support this observation. The OH^- groups in the crystal structure of the CGM replace oxygen in the O7 position and are bound in the tetrahedral M2 cations (position T in the formula),[13] so that the cations with the 6*c* Wyckoff position form bonds with O–H. If considering structural data of natural loveringite,[15] this cation group is an inactive Raman mode, though using structural data of synthetic one,[53] the 6*c* cations should produce Raman-active modes in spectra. In the latter case, the absence of O–H stretching vibrations in the CGM Raman spectra should be explained in different way. Whether or not, structural analysis shows M0–M2 cationic groups to be active in the IR and, as a result, structural water bands should occur in the IR spectra. With that, the presence of hydroxyl in the CGM can also explain the low totals of EMP analyses. In addition, it should be noted that the CGM structure allows for a significant amount of vacancies,[53] which was later supported by a natural sample study (e.g., Ge et al[14]). Moreover, the crystal structure of the CGM is known to have additional M-sites (M6–M9; e.g., other studies[1,2,12]), to where cations can be distributed, though only one of neighboring sites can commonly be inhabited. The presence of vacancies and extra sites probably might explain the low totals too, even when performing high quality EMP analysis not contaminated by the host mineral matrix.

6.4 | Implications for mantle petrology

An exhausitive examination of CGM as inclusions in mantle minerals or as discrete grains in mantle samples is important from the genetic and petrological points of view. The chemical composition of CGM interconnects to *P–T–X* parameters during crystallization.[18,53,59] The CGM are stable at P–T–fO_2 mantle conditions,[18,53,60] and as it was shown experimentally, the larger-ion varieties, mathiasite and lindsleyite, can be stable at pressures and temperatures corresponding to the diamond stability field.[18] The latter finds natural proofs by occurrence of crichtonite and akin magnetoplumbite group minerals included into diamond[61-64] testifying their high *P–T* sustainability. Together with that, the coexistence of CGM and minerals with oxidized and reduced form of carbon, namely carbonates (magnesite) and graphite, as inclusions in garnet,[22] may shed light into the role of metasomatism in the deep carbon cycle. The Mn- and REE-rich loveringite-like compounds have been synthesized at 2–3 GPa and 1,000° C–1,300° C[53,60] and are known to be stable under strongly reduced conditions ($\log fO_2$ ranges from –15 to –18).[53] With respect to the redox regime of the mantle, it highlights an interest to a transition metals valence state study applied to natural CGM.

An examination of various inclusions in mantle minerals allows to access the mantle processes responsible

for genesis and transformation of deep-seated rocks (e.g., other studies[24,41,42,45,61,64]). Complex alkali- and large ion lithophile element-bearing titanates of the crichtonite group along with magnetoplumbite group minerals (e.g., other studies[41,62,65]) are commonly reported as metasomatic oxides from the subcontinental mantle settings, both on- and off-cratonic. The members of both groups are present in xenoliths and/or as xenocrysts sampled by kimberlites, lamprophyres, and alkali basalts.[16,34,37,64,66-71] Regarding the Siberian craton, CGM are known as individual inclusions in pyropic garnet xenocrysts from Yakutian kimberlites, that is, Internatsionalnaya,[24,39,72] Zagadochnaya,[73] Sytykanskaya,[74] as well as from ultramafic rocks of the Chompolo and Tobuk-Khatystyr volcanic fields, Aldan shield.[22,72,74] They are described in a series of oriented needles within garnet grains of mantle xenoliths from Udachnaya, Obnazhennaya, and Mir kimberlites.[40,45] Enstatite-hosted CGM inclusions have been recently recognized in an orthopyroxenite from Udachnaya.[41,75] The CGM-bearing samples from Siberia are known to have been equilibrated at pressures of 2.5–4.2 GPa and temperatures of 650° C–850 ° C.[22,24,39-41,73] Mantle CGM are considered to be a valuable reservoir of a large number of high field strength, large ion lithophile, and REE with their abundance up to ~100 chondritic units.[10,16,26,76] This fact together with CGM stability at high pressures and temperatures makes them potentially important repository for rock-forming mantle silicate-incompatible trace elements, together with well-known metasomatic minerals—phlogopite, amphibole, and carbonates—and, thus, provides clues to fluid and magma generation at upper-mantle conditions and metasomatism of the depleted lithospheric mantle.

7 | CONCLUSIONS

Micro-Raman spectroscopy may be used as a helpful tool for the verification of the CGM analyzed with EMP and SEM, especially when measuring small grains and inclusions or fine mineral intergrowths.

1. The CGM can be easily identified by means of Raman spectroscopy. Using thin slices of measured minerals with translucent edges, lower laser beam power and laser wavelength all assist in recording qualitative spectra.
2. Crystal structure refinement applied to mantle loveringite and its Sr-, Ba-, and Na-bearing analogues, as well as to Cr-rich species, is highly required to decipher the Raman spectra of these minerals.
3. The Raman spectra of CGM are perplexed by overlapping bands of different groups. However, the major contributors (mostly TiO_6 and to a lower extent CrO_6, MgO_4, and FeO_4 groups) become evident in distinct bands. The strongest Raman bands located at 130, 300–310, 410–440, 710–720, and 810–820 cm^{-1} allow distinguishing CGM.
4. The major influence on the position of the Raman bands is attributed to elements occupying M2–M5 positions (C and T). The impact of the M0 and M1 sites on the Raman bands is negligible, yet the influence of the elements occurring in these polyhedra is predicted to be significant in the IR spectra. The OH^- group is anticipated to be active in infrared absorption.

ACKNOWLEDGEMENTS

This study was supported by the Russian Science Foundation (Grant 18-77-10062). The equipment of the Ural Center for Shared Use «Modern Nanotechnology», Ural Federal University, and the Analytical Center for Multi-elemental and Isotope Research, IGM, was used. Sampling was supported by the Russian Federation state assignment project of IGM. We are grateful to Nikolai V. Sobolev for Samples O-173, O-39, and O-264. Vladimir N. Korolyuk, Elena N. Nigmatulina (IGM), and Allan Patchen (UT) are highly appreciated for the help with EMP analyses. We express our sincere thanks to F. Nestola and an anonymous reviewer for their thorough reviews and helpful suggestions, and to C. Marshall for regardful editorial handling of the manuscript on every stage of its revision.

ORCID

Taisia Alifirova https://orcid.org/0000-0001-9154-7797
Dmitriy Rezvukhin https://orcid.org/0000-0001-7421-6507
Evgeny Nikolenko https://orcid.org/0000-0003-1556-6026
Pavel Zelenovskiy https://orcid.org/0000-0003-3895-4785
Andrey Korsakov https://orcid.org/0000-0002-4922-7658

REFERENCES

[1] T. Armbruster, M. Kunz, *Eur. J. Mineral.* **1990**, *2*, 163.
[2] P. Orlandi, M. Pasero, G. Duchi, F. Olmi, *Am. Mineral.* **1997**, *82*, 807.
[3] I. E. Grey, D. J. Lloyd, J. S. White, **1976**, *61*, 1203.
[4] P. A. Wülser, N. Meisser, J. Brugger, K. Schenk, S. Ansermet, M. Bonin, F. Bussy, *Eur. J. Mineral.* **2005**, *17*, 933.
[5] P. A. Wülser, J. Brugger, N. Meisser, *Bull. Liaison Soc. Fr. Minéral. Cristallogr* **2004**, *16*, 76.

[6] I. E. Grey, B. M. Gatehouse, *Can. Mineral.* **1978**, *16*, 63.
[7] B. M. Gatehouse, I. E. Grey, *Am. Mineral.* **1979**, *64*, 1010.
[8] R. L. Frost, B. J. Reddy, *Rad. Effects Defects Solids* **2011**, *166*, 131.
[9] E. Bittarello, M. E. Ciriotti, E. Costa, L. M. Gallo, *Int. J. Mineral.* **2014**, *14*, 6.
[10] A. P. Jones, V. Ekambaram, *Am. Mineral.* **1985**, *70*, 414.
[11] S. J. Mills, L. Bindi, M. Cadoni, A. R. Kampf, M. E. Ciriotti, G. Ferraris, *Eur. J. Mineral.* **2012**, *24*, 1061.
[12] C. Biagioni, P. Orlandi, M. Pasero, F. Nestola, L. Bindi, *Eur. J. Mineral.* **2014**, *26*, 427.
[13] L. A. Filho, N. V. Chukanov, R. K. Rastsvetaeva, S. M. Aksenov, I. V. Pekov, M. L. Chaves, R. P. Richards, D. Atencio, P. R. Brandão, R. Scholz, *Mineral. Mag.* **2015**, *79*, 269.
[14] X. Ge, G. Fan, G. Li, G. Shen, Z. Chen, Y. Ai, *Eur. J. Mineral.* **2017**, *29*, 331.
[15] B. M. Gatehouse, I. E. Grey, I. H. Campbell, P. Kelly, *Am. Mineral.* **1978**, *63*, 28.
[16] S. E. Haggerty, *Geochim. Cosmochim. Acta* **1983**, *47*, 1833.
[17] J. Zhang, J. Ma, L. Li, *Geol. Rev.* **1988**, *34*, 132.
[18] J. Konzett, H. Yang, D. J. Frost, *J. Petrol.* **2005**, *46*, 749.
[19] B. M. Gatehouse, I. E. Grey, J. R. Smyth, *Acta Crystallog. Sec. C* **1983**, *C39*, 421.
[20] R. G. Platt, R. H. Mitchell, *Mineral. Mag.* **1996**, *60*, 403.
[21] E. G. Potter, R. H. Mitchell, *Contrib. Mineral. Petrol.* **2005**, *150*, 212.
[22] E. I. Nikolenko, I. S. Sharygin, T. A. Alifirova, A. V. Korsakov, P. S. Zelenovskiy, V. Y. Shur, *J. Raman Spectros.* **2017**, *48*, 1597.
[23] A. Y. Barkov, M. E. Fleet, R. F. Martin, Y. P. Shikov'Men, *Eur. J. Mineral.* **2006**, *18*, 493.
[24] D. I. Rezvukhin, V. G. Malkovets, I. S. Sharygin, I. G. Tretiakova, W. L. Griffin, S. Y. O'Reilly, *Lithos* **2018**, *308*, 181.
[25] B. Lafuente, R. T. Downs, H. Yang, N. Stone, *Highlights in mineralogical crystallography*, Walter de Gruyter GmbH, Berlin, **2016**, 1.
[26] M. Grégoire, D. Bell, A. L. Roex, *Contrib. Mineral. Petrol.* **2002**, *142*, 603.
[27] C. Ma, J. R. Beckett, H. C. Connolly, G. R. Rossman, in Lunar and Planetary Science Conference, Vol. *44*, The Woodlands, Texas, U.S.A. **2013**, 1443.
[28] R. C. Rouse, D. R. Peacor, *Am. Mineral. J. Earth Planet. Mater.* **1968**, *53*, 869.
[29] M. E. Fleet, C. M. D. Almeida, N. Angeli, *Can. Mineral.* **2002**, *40*, 341.
[30] D. J. Mossman, *Can. Mineral.* **1985**, *23*, 495.
[31] R. Cabella, M. Gazzotti, G. Lucchetti, *Can. Mineral.* **1997**, *35*, 899.
[32] A. Giuliani, D. Phillips, R. Maas, J. D. Woodhead, M. A. Kendrick, A. Greig, R. A. Armstrong, D. Chew, V. S. Kamenetsky, M. L. Fiorentini, *Earth Planet. Sci. Lett.* **2014**, *401*, 132.
[33] G. Săbău, A. Alberico, *Studia Univ. Babes-Bolyai Geologia* **2007**, *52*, 55.
[34] V. Almeida, V. Janasi, D. Svisero, F. Nannini, *Open Geosci.* **2014**, *6*, 614.
[35] W. L. Gong, R. C. Ewing, L. M. Wang, H. S. Xie, *MRS Online Proc. Library Arch.* **1994**, *353*, 807.
[36] W. J. Buykx, K. Hawkins, D. M. Levins, H. Mitamura, R. S. C. Smart, G. T. Stevens, K. G. Watson, D. Weedon, T. J. White, *J. Am. Ceram. Soc.* **1988**, *71*, 678.
[37] L. Wang, E. J. Essene, Y. Zhang, *Contrib. Mineral. Petrol.* **1999**, *135*, 164.
[38] S. E. Haggerty, *Rev. Mineral. Geochem.* **1991**, *25*, 355.
[39] D. I. Rezvukhin, V. G. Malkovets, I. S. Sharygin, D. V. Kuzmin, A. A. Gibsher, K. D. Litasov, N. P. Pokhilenko, N. V. Sobolev, *Dokl. Earth Sci.* **2016**, *466*, 206.
[40] T. A. Alifirova, L. N. Pokhilenko, Y. I. Ovchinnikov, C. L. Donnelly, A. J. V. Riches, L. A. Taylor, *Int. Geol. Rev.* **2012**, *54*, 1071.
[41] D. I. Rezvukhin, T. A. Alifirova, A. V. Korsakov, A. V. Golovin, *Am. Mineral.* **2019**, *104*, 761.
[42] K. Sakamaki, Y. Sato, Y. Ogasawara, *Prog. Earth Planet. Sci.* **2016**, *3*, 20.
[43] P. Orlandi, M. Pasero, N. Rotiroti, F. Olmi, F. Demartin, Y. Moëlo, *Eur. J. Mineral.* **2004**, *16*, 171.
[44] N. V. Sobolev, E. S. Yefimova, *Int. Geol. Rev.* **2000**, *42*, 758.
[45] D. Spengler, T. A. Alifirova, *Lithos* **2019**, 326.
[46] G. P. Brey, T. Köhler, *J. Petrol.* **1990**, *31*, 1353.
[47] P. Nimis, H. Grütter, *Contrib. Mineral. Petrol.* **2010**, *159*, 411.
[48] H. Grútter, D. Latti, A. Menzies, *J. Petrol.* **2006**, *47*, 801.
[49] D. L. Whitney, B. W. Evans, *Am. Mineral.* **2010**, *95*, 185.
[50] H. S. Grütter, J. J. Gurney, A. H. Menzies, F. Winter, *Lithos* **2004**, *77*, 841.
[51] A. J. Locock, *Comput. Geosci.* **2008**, *34*, 1769.
[52] E. Kroumova, M. I. Aroyo, J. M. Perez-Mato, A. Kirov, C. Capillas, S. Ivantchev, H. Wondratschek, *Phase Transit.* **2003**, *76*, 155.
[53] R. C. Peterson, I. E. Grey, L. M. D. Cranswick, C. Li, *Can. Mineral.* **1998**, *36*, 763.
[54] A. Wang, B. L. Jolliff, K. E. Kuebler, L. A. Haskin, *Am. Mineral.* **2004**, *89*, 665.
[55] M. Wojdyr, *J. Appl. Crystallography* **2010**, 1126.
[56] T. Laetsch, R. T. Downs, in 19th General Meeting of the International Mineralogical Association, Vol. *23*, Kobe, Japan, **2006**, 28.
[57] B. A. Kolesov, C. A. Geiger, *Phys. Chem. Miner.* **1998**, *25*, 142.
[58] C. Lenz, L. Nasdala, D. Talla, C. Hauzenberger, R. Seitz, U. Kolitsch, *Chem. Geol.* **2015**, *415*, 1.
[59] S. Foley, H. Höfer, G. Brey, *Contrib. Mineral. Petrol.* **1994**, *117*, 164.
[60] T. H. Green, N. J. Pearson, *Mineral. Mag.* **1987**, *51*, 145.
[61] N. V. Sobolev, E. S. Yefimova, F. V. Kaminsky, L. V. Usova, in Composition and Processes of Deep-Seated Zones of Continental lithosphere: International Symposium, Novosibirsk **1988**, 185.
[62] N. V. Sobolev, F. V. Kaminsky, W. L. Griffin, E. S. Yefimova, T. T. Win, C. G. Ryan, A. I. Botkunov, *Lithos* **1997**, *39*, 135.
[63] I. Leost, T. Stachel, G. P. Brey, J. W. Harris, I. D. Ryabchikov, *Contrib. Mineral. Petrol.* **2003**, *145*, 15.
[64] G. P. Bulanova, E. Muchemwa, D. G. Pearson, B. J. Griffin, S. P. Kelley, S. Klemme, C. B. Smith, *Lithos* **2004**, *77*, 181.
[65] S. E. Haggerty, A. J. Erlank, I. E. Grey, *Nature* **1986**, *319*, 761.
[66] A. P. Jones, J. V. Smith, J. B. Dawson, *J. Geology* **1982**, *90*, 435.

[67] F. Kalfoun, D. Ionov, C. Merlet, *Earth Planet. Sci. Lett.* **2002**, *199*, 49.
[68] A. J. Erlank, F. G. Waters, C. J. Hawkesworth, S. E. Haggerty, H. L. Allsopp, R. S. Rickard, M. A. Menzies, *in Mantle Metasomatism*, Academic Press, London **1987**, 221.
[69] P. H. Nixon, E. Condliffe, *Mineral. Mag.* **1989**, *53*, 305.
[70] D. Velde, *Am. Mineral.* **2000**, *85*, 420.
[71] S. Vrana, *J. Geosci.* **2008**, *53*, 17.
[72] S. I. Kostrovitsky, V. K. Garanin, in International Kimberlite Conference: Extended Abstracts, Vol. *5*, Rio de Janeiro, Brazil **1991**, 525.
[73] L. Ziberna, P. Nimis, A. Zanetti, A. Marzoli, N. V. Sobolev, *J. Petrol.* **2379**, *2013*, 54.
[74] A. Varlamov, V. K. Garanin, S. I. Kostrovitskiy, *Dokl. Akad. Nauk* **1995**, *345*, 364.
[75] D. I. Rezvukhin, T. A. Alifirova, A. V. Golovin, A. V. Korsakov, *Minerals* **2020**, *10*, 264.
[76] J. Konzett, R. A. Armstrong, D. Günther, *Contrib. Mineral. Petrol.* **2000**, *139*, 704.

SUPPORTING INFORMATION

Additional supporting information may be found online in the Supporting Information section at the end of this article.

How to cite this article: Alifirova T, Rezvukhin D, Nikolenko E, et al. Micro-Raman study of crichtonite group minerals enclosed into mantle garnet. *J Raman Spectrosc*. 2020;51: 1493–1512. https://doi.org/10.1002/jrs.5979